Supramolecular Hydrogel Induced by Electrostatic Interactions between Polycation and Phosphorylated-Fmoc- tripeptide

Miryam Criado-Gonzalez, Déborah Wagner, Jennifer Rodon Fores, Christian Blanck, Marc Schmutz, Alain Chaumont, Morgane Rabineau, Joseph B Schlenoff, Guillaume Fleith, Jérôme Combet, et al.

Supramolecular Hydrogel Induced by Electrostatic Interactions between Polycation and Phosphorylated-Fmoc-tripeptide

Miryam Criado-Gonzalez,[a,b,c,‡] Déborah Wagner,[a,‡]Jennifer Rodon Fores,[a] Christian Blanck,[a] Marc Schmutz,[a] Alain Chaumont [d], Morgane Rabineau[b,c], Joseph B. Schlenoff,[e] Guillaume Fleith,[a] Jérôme Combet [a], Pierre Schaaf,*[,a,b,c,f] Loïc Jierry,[a,f] Fouzia Boulmedais*[,a]

a. Université de Strasbourg, CNRS, Institut Charles Sadron UPR 22, 67034 Strasbourg, France.

b. Institut National de la Santé et de la Recherche Médicale, UMR-S 1121, "Biomatériaux et Bioingénierie", 67087 Strasbourg, France.

c. Université de Strasbourg, Faculté de Chirurgie Dentaire, Fédération de Médecine Translationnelle de Strasbourg and Fédération des Matériaux et Nanoscience d'Alsace, 67000 Strasbourg, France.

d. Université de Strasbourg, Faculté de Chimie, UMR7140, 67000 Strasbourg, France.

e. Department of Chemistry and Biochemistry, Florida State University, Tallahassee, Florida 32306, United States

f. Université de Strasbourg, Ecole de Chimie, Polymères et Matériaux, Strasbourg, France.

ABSTRACT: Supramolecular hydrogels formed through non-covalent interactions of low molecular weight hydrogelators (LMWH) show great potential applications in different fields, such as delivery of therapeutics, injectable biomaterials, catalysis or materials chemistry. Generally, the self-assembly of LMWH is triggered by a sol-gel process through an external stimulus able to switch their solubility, such as temperature, pH or solvent change and chemical or enzymatic reactions. In this work, we introduced a new strategy to trigger and control the self-assembly of Fmoc-FFpY peptides: by direct electrostatic interactions with a polycation without dephosphorylation of the peptides. The resulting hydrogels show enhanced mechanical properties in comparison to gels of Fmoc-FFpY induced by enzymatic dephosphorylation. Peptide self-assembly yields β-sheets, revealed by circular dichroism and infrared spectroscopy. Characteristic distances predicted by geometry optimization in the gas phase are in agreement with X-ray scattering data and TEM observations. It is proposed that core-shell cylinders are formed in which polycation chains decorate the micellar structures of Fmoc-FFpY peptides through electrostatic interactions between the charged amine groups of the polycations and the phosphate groups of the peptides. Since the gels form quickly and have superior mechanical properties, applications as injectable biomaterials are foreseen. This work opens a route towards a new class of self-assembled hydrogels, where Fmoc tripeptides can be self-assembled with specific polycations to obtain, for example, antimicrobial hydrogels.

Introduction

Supramolecular hydrogels formed through non-covalent interactions of low molecular weight hydrogelators (LMWH) show great potential applications in different fields, such as biomedicine,[1-2] catalysis[3-4] and materials chemistry[5]. Self-assembling peptides have been explored for the encapsulation and delivery of therapeutics over the past decades thanks to their biocompatibility, biodegradability and low toxicity.[6-7] The use of reversible non-covalent bonds affords new materials with dynamic responses towards external stimuli, endowing them with the capability to adapt to the surrounding environment.[8-10] Injectable hydrogels, based on polymers or peptides, have drawn considerable attention as implants because of their minimal invasive implantation.[11-12] Generally, the self-assembly of LMWH is triggered by a sol-gel process through an external stimulus able to switch their solubility.[13] Typical stimuli include temperature change,[14] pH switch,[15-16] solvent change,[17] chemical reactions[18-19] and enzymatic reactions[20-22]. The use of small peptides with a sequence-defined chemical structure gives hydrogels with a desired functionality.[23] Among these small peptides, those bearing fluorenylmethyloxycarbonyl (Fmoc) groups and containing phenylalanine amino acids have recently attracted great attention due to their high propensity to self-assemble through π-π interactions between aromatic groups.[24-25] Because they are poorly soluble in water, peptides are usually induced to self-assemble by dissolution in DMSO followed by a dilution step in water,[26] by change of pH[25] and/or by heating the solution, often up to 80°C for solubilization, followed by a cooling step.[27-28] To circumvent this drawback, the enzyme assisted self-assembly (EASA) of peptides was introduced by the seminal work of Xu and coworkers.[20-21] Phosphorylated Fmoc-peptides, soluble at room temperature in aqueous solution, were transformed into gelators by alkaline phosphatase (AP) catalyzed removal of phosphate groups. Later, we introduced the use of non-self-assembling Fmoc-FFpY peptide (F: phenylalanine; Y: tyrosine; p: PO_4^{2-}), which is transformed into the hydrogelator Fmoc-FFY by AP, to localize EASA on a surface using a seed layer.[29] The mechanical properties of Fmoc-FFY gels are poor (modulus ~ 10 Pa) limiting their potential applications. In addition, the self-assembly of Fmoc-FFY in a covalent gel[22] and from AP functionalized silica nanoparticles do not change

the mechanical properties.[30] Co-assembly of similar long and short peptides enhanced the mechanical property of the resulting hydrogel. This was done with an ionic-complementary octapeptide, alternating positive and negative charged amino acids, to form a controllable number of cross-links/branch points in the β-sheet fibrillar network.[31] The combination of peptides and polymers overcomes such limitations through covalent linking or non-covalent interactions.[32] In the latter case, via electrostatic interactions, the co-assembly of long peptides (> 10 amino acids), such as amphiphilic peptides or multi-domain peptides (*i.e.* peptide with alternated hydrophobic and hydrophilic residues terminated by charged residues) with oppositely charged polyelectrolytes led rather to sacs,[33] membranes,[34-35] microcapsules[36] or microparticles.[37] A few gels were obtained, by co-assembly of poly(styrene sulfonate) with positively charged amphiphilic peptides[38] or heparin with positively charged multi-domain peptides.[39-40] In the case of short peptides, a hybrid hydrogel was obtained by combining negatively charged Fmoc-FF (bearing a C terminal COOH group) and poly(L-lysine). One main drawback of this system is that gel formation required 3 days of aging.[41-42] In all these studies, the presence of the polyelectrolyte chains affects but never induces the peptide self-assembly. Indeed, the peptide can self-assemble in the absence of polyelectrolyte chains. In this work, we introduce a new strategy to trigger and control the self-assembly of Fmoc-FFpY peptides. The formation of the peptidic hydrogel is obtained instantaneously by direct electrostatic interactions with a polycation without dephosphorylation of the peptides (Scheme 1).

Scheme 1. Representation of PAH/Fmoc-FFpY supramolecular hydrogel a) Electrostatic interaction between Fmoc-FFpY and PAH leading to the (b) formation of PAH/Fmoc-FFpY hydrogel by simple mixture between PAH and Fmoc-FFpY solutions.

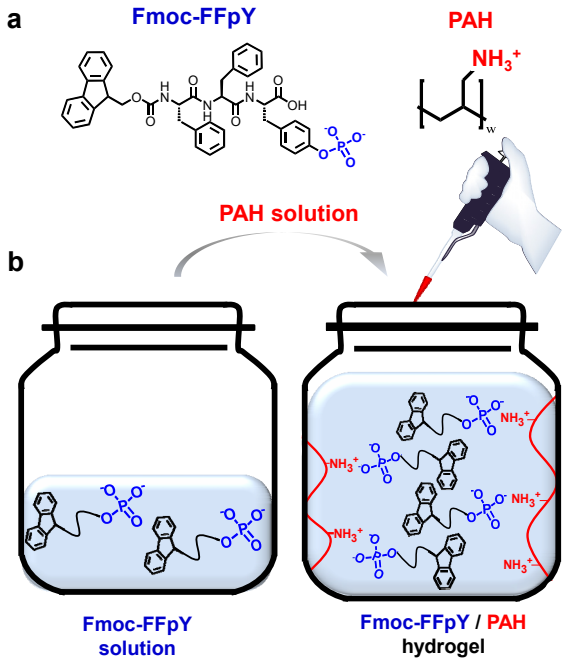

Here, self-assembly is promoted by a dual mechanism based on (i) supramolecular interactions between Fmoc-FFpY peptides and (ii) electrostatic interactions between the peptides and the oppositely charged polyelectrolyte chains.

Materials and Methods

Materials. Poly(allylamine hydrochloride) (PAH, Mw = 120 000 g/mol) was from Alfa Aesar. Fmoc-FFpY was purchased from PepMic. Alkaline Phosphatase (AP, 10 DEA units/mg protein) from bovine intestinal mucosa, Thioflavin T, poly(diallyldimethylammonium chloride) (PDADMA, Mw = 100 000 g/mol, 35% wt in H_2O) and PAH (Mw = 58 000 g/mol) were from Sigma Aldrich. p-Nitrophenyl phosphate (PNP) was from ThermoFisher Scientific. Sodium tetraborate anhydrous (borax) was supplied by Acros Organics. Poly(L-lysine hydrobromide) (PLL) (Mw = 52 000 g/mol) and Poly(L-arginine hydrochloride) (PAR) (Mw = 9 600 g/mol) were from Alamanda.

Inversion tests. Unless otherwise stated, solutions were prepared at 107.5 mM in polycation monomer and 12.9 in mM Fmoc-FFpY using 25 mM borax buffer at pH 9.5 and MilliQ water. Inversion tests were carried out by adding 100 µL of polycation solution to 100 µL of Fmoc-FFpY in a vial. After mixing them few seconds, the vial was inverted.

Viscoelastic Properties. Hydrogels were prepared in Teflon molds of 10 mm diameter by mixing 150 µL of Fmoc-FFpY solution with 150 µL of PAH solution to obtain final concentrations of 10 mg/mL PAH and 10 mg/mL Fmoc-FFpY. Fmoc-FFY gel was obtained at 1.5 mg/mL AP and 10 mg/mL Fmoc-FFpY concentrations. After 24 h gelation, viscoelastic properties were measured in a Kinexus Malvern rheometer using a plate (sandblasted) geometry of 10 mm diameter and a gap of 2 mm. Strain measurements were carried out from 0.01% to 100% at 1 Hz and frequency sweeps were performed from 0.01 Hz to 10 Hz at 1% strain at 25 °C.

Confocal Microscopy. Confocal laser scanning microscopy images were captured with a Zeiss LSM 710 microscope using EC Plan-Neofluar 10x/0.3, Plan-Apochromat 20x/0.8 M27 and EC Plan-Neofluar 40x/0.75 M27 objectives. PAH was labelled by rhodamine (PAHr) using a standard protocol.[43] The fluorescence of rhodamine was measured with an excitation wavelength of 561 nm and emission between 566 and 703 nm. The self-assembly was visualized by adding thioflavine T (1 mg/mL) in the peptide solution. The fluorescence of thioflavine T was measured with excitation by an argon laser with a cut-off dichroic mirror at 488 nm and an emission band-pass filter between 493 and 548 nm. Gels were prepared as described earlier but with thioflavin T (1 mg/mL) added in Fmoc-FFpY solution.

Fourier Transform Infrared spectroscopy (FTIR). FTIR experiments were performed on a Vertex 70 spectrometer (Bruker, Germany) using a DTGS detector. Spectra were recorded in the Attenuated Total Reflection (ATR) mode using a single reflection diamond ATR by averaging 128 interferograms between 600 and 4000 cm^{-1} at 2 cm^{-1} resolution, using Blackman-Harris three-term apodization and Bruker OPUS/IR software (version 7.5). Samples were prepared in D_2O with Borax buffer at pH 9.5. PAH/Fmoc-FFpY gel was obtained at 10 mg/mL PAH and 10 mg/mL Fmoc-FFpY concentrations. Fmoc-FFY gel was obtained at 1.5 mg/mL AP and 10 mg/mL Fmoc-FFpY concentrations. To decompose the amide I band, data processing was performed using OPUS 7.5 software (Bruker Optik GmbH). The spectra were smoothed using a twenty-five point smoothing function, cut between 1550 and 1710 cm^{-1} and then normalized using a normalization "min-max" method. The baseline was then adjusted to calculate the second or the fourth derivative. The number and the frequencies of the different components, forming the amide I band,

and the other peaks were determined by means of the fourth derivative of the Fourier smoothed spectrum, using the maximum positions. The fourth derivative was used to determine the position of the peaks as it is suggested in the case for highly overlapped components.[44] The decomposed spectrum was fitted with Gaussian band profiles using local least squares followed by Levenberg-Marquart's method, starting with intensities of 0.1 and widths of 5. The quality of the fitting was estimated by the residual RMS provided by the software. The relative contribution of each component of the amide I band was calculated by the ratio of the area of each peak over the area of the total amide I band.

Fluorescence spectroscopy. All fluorescence spectra were recorded between 300-900 nm using a Fluoromax-4 (Horiba Jobin Yvon - Edison, NJ USA) at an excitation wavelength of 290 nm and a quartz cuvette of 1 mm path length. Baselines were acquired with Borax buffer. PAH/Fmoc-FFpY gel was obtained at 0.5 mg/mL PAH and 0.5 mg/mL Fmoc-FFpY concentrations. Fmoc-FFY gel was obtained at 1 mg/mL AP and 0.5 mg/mL Fmoc-FFpY concentrations. Before using PAH, impurities that interfered with fluorescence measurements were removed by the following protocol: PAH was dissolved in methanol followed by precipitation in cold ether, two centrifugations at 6 000 rpm for 5 min and drying under vacuum for 12 h to recover the polymer.

Circular dichroism (CD). CD spectra were recorded between 190 and 800 nm using a Jasco J-1100 spectropolarimeter with a data pitch of 1 nm on the light wavelength. The baseline was acquired with Borax buffer. PAH/Fmoc-FFpY gel was obtained at 0.5 mg/mL PAH and 0.5 mg/mL Fmoc-FFpY. Fmoc-FFY gel was obtained at 1 mg/mL AP and 0.5 mg/mL Fmoc-FFpY.

Analytic High-Performance Liquid Chromatography (HPLC). HPLC was carried out with an Agilent 1100 Series system. The column was a Supelcosil ABZ + Plus 15 cm × 4.6 mm with 3 µm stationary phase. The eluent for all analyses was 90/10 acetonitrile/deionized water in isocratic conditions, at 1 mL/min with a run time of 25 min. Chromatograms were recorded using OpenLab Agilent 1100 software. PAH/Fmoc-FFpY gel was obtained at 10 mg/mL PAH and 10 mg/mL Fmoc-FFpY. Fmoc-FFY gel was obtained at 1.5 mg/mL AP and 10 mg/mL Fmoc-FFpY. The gel (1 mL in volume) was diluted in 1.5 mL of acetonitrile, vortexed and filtered on 0.2 µm PTFE before injection into the column.

Transmission Electron Microscopy (TEM). TEM images were taken in a Technai G2 machine with negative staining. 5 µL of PAH/Fmoc-FFpY gel, or Fmoc-FF gel, were dropped on a carbon-coated copper grid for observation. PAH/Fmoc-FFpY gel was obtained at 5 mg/mL PAH and 5 mg/mL Fmoc-FFpY Fmoc-FFY gel was obtained at 1 mg/mL AP and 5 mg/mL Fmoc-FFpY.

Small and wide angle X-ray scattering (SAXS-WAXS). Small and wide angle X-ray scattering experiments (SAXS-WAXS) were performed on a Rigaku diffractometer operating with a microfocus rotating anode generator (Micromax-007 HF, 40kV 30 mA, Cu-Kα radiation, λ=1.54 Å). The X-ray beam was monochromatized and focused with Confocal Max-Flux optics (Osmic) fitted with a three-pinhole collimation system. The beamstop was equipped with a PIN-diode to determine the transmission factor. In the SAXS configuration, the intensity was collected with a 2D multiwires camera located 0.81 m from the sample and covering a scattering vector range 0.011 $Å^{-1} < q < 0.33$ $Å^{-1}$ (q is defined as $4\pi/\lambda \sin(\theta/2)$ where θ is the scattering angle). WAXS measurements were carried out using Fuji imaging plates installed 0.1 m from the sample and extending the available q range to 3 $Å^{-1}$. Samples were introduced between thin calibrated mica cells (1 mm apart). Intensities were corrected according to usual procedures. Data were radially integrated, corrected for electronic background, detector efficiency, empty cell scattering, thicknesses and transmission factors. Scattering from pure solvent was recorded and removed from the sample measurements. The q-range was calibrated with powder diffraction peaks from silver behenate. Intensity was converted into absolute scales using a Lupolen standard. The finite instrumental resolution was evaluated from the width of the diffraction peaks of tricosane powder and was considered to be constant in the q-range of interest. All measurements were carried out at room temperature. Experiments were repeated twice on different equivalent samples. The typical counting time was 14 h in the SAXS setup, and 4 h for the WAXS configuration. PAH/Fmoc-FFpY gel was obtained at 5 mg/mL PAH and 5 mg/mL Fmoc-FFpY.

Modelling of SAXS curve. The corrected intensity $I(q)$ represents the total scattering cross section per unit volume and contains all the information about the structural organization of the solute. For monodisperse non-interacting particles in a media, it can be written

$$I(q) = \Phi \frac{P(q)}{V}$$

where ϕ is the volume fraction of the particles, V their volume and $P(q)$ their form factor. $P(q)$ is related to the shape and the size of the scattering objects and can modeled on the basis of simple geometrical descriptions. In the present study, only cylindrical models are considered. For long core-shell isolated cylinders ($L_{\text{cylinder}} >> 10\ R_{\text{cylinders}}$), the theoretical form factor and the intensity are given by

$$\begin{cases} P(q,R_2,R_1,L) = \dfrac{4\pi^3 L}{q^3}\left[R_1(\rho_1-\rho_S)J_1(qR_1) + R_2(\rho_2-\rho_1)J_1(qR_2)\right]^2 \\ V = \pi {R_1}^2 L \\ I(q) = \Phi \dfrac{4\pi^2}{{R_1}^2 q^3}\left[R_1(\rho_1-\rho_S)J_1(qR_1) + R_2(\rho_2-\rho_1)J_1(qR_2)\right]^2 \end{cases}$$

where L is the length of the cylinders, R_1 and R_2 are the external and internal (core) radii, and ρ_1, ρ_2 and ρ_S are the scattering length densities of the shell, the core and the solvent respectively. The shell thickness e is given by (R_1 - R_2). J_1 is the Bessel function of first kind and first order. When R_2=0, the core disappears and we recover the form factor of a classical cylinder (homogeneous scattering length density). When parallel cylinders are in contact (associated cylinders model), the previous intensity is simply multiplied by an interference term:

$$I(q) = \Phi \frac{P(q)}{V}(1 + J_0(2qR_1))$$

where J_0 is the Bessel function of first kind and zero order.

Fitting procedure of SAXS curve. Experimental normalized intensity was compared to theoretical scattering calculated for different model structures (single/associated core-shell/homogenous cylinders) using IGOR Pro and analysis macros developed by the NIST Center for Neutron Research[45] (Figure S10-13 in SI). Theoretical intensities were smeared by the instrumental resolution before comparison to the experimental data.

A Gaussian polydispersity was applied to the internal radius R_2 while keeping the shell thickness e constant:

$$g(R_2) = \frac{1}{\Delta R_2 \sqrt{2\pi}} \exp\left(-\frac{(R_2 - \overline{R_2})^2}{2\Delta R_2^{\,2}} \right)$$

where $\overline{R_2}$ is the average internal radius and ΔR_2 is the standard deviation.

The fitting parameters were the external and internal radii (R_1, R_2), the external and internal scattering length densities (ρ_1, ρ_2) and the standard deviation ΔR_2. The volume fraction Φ was allowed to slightly vary around its theoretical value to overcome uncertainties in the absolute scale calibration. The scattering length density of the solvent ρ_s was fixed to that of pure water (9.40 10^{-10} cm^{-2}). A flat background contribution (bkg) was finally added to the model. Only a restricted q-range was considered during the fitting procedure and never exceeded q = 0.35 $Å^{-1}$.

Quantum calculations / Gas Phase Geometry optimization. A cluster composed by 4 Fmoc-FFpY and 2 PAH was constructed from scratch and initially placed in the desired geometry using Avogadro 1.2.0 software.[46] The system was then relaxed to a stable state by geometry optimization calculations at the Hartree Fock level using a 6-31G basis set. Geometry optimization was performed with the Gaussian09 Rev D.01. software.[47]

Results and Discussion

Characterization of PAH/Fmoc-FFpY hydrogel. The Fmoc-FFpY peptide is known to transform into Fmoc-FFY in the presence of AP which then self-assembles to form a gel.[48] Here, we show that the hydrogelation of Fmoc-FFpY can occur by electrostatic interactions with polycation chains without dephosphorylation whereas Fmoc-FFpY solution by itself does not gel even after several days. A phase diagram was established using the inverted tube test, a commonly-accepted method for screening whether a gel has been formed (Figure S1a in Supporting Information, SI).[49] A gel forms instantly by mixing PAH and Fmoc-FFpY at 10 mg/mL in borax buffer at pH 9.5 (Figure 1).

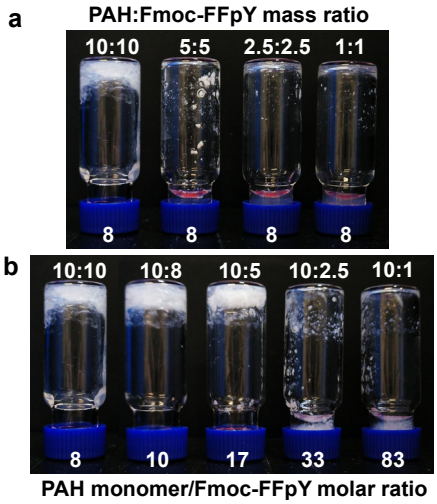

Figure 1. Inverted vial tests of PAH/Fmoc-FFpY hydrogels obtained by mixing (a) PAH (Mw= 120 000 g/mol) and Fmoc-FFpY solutions at different concentrations keeping constant PAH monomer/Fmoc-FFpY molar ratio at 8 and (b) PAH (Mw= 120 000 g/mol) at 10 mg/mL and Fmoc-FFpY at different concentrations to obtain different PAH monomer/Fmoc-FFpY molar ratios.

By keeping the molar ratio of PAH monomer/Fmoc-FFpY constant at 8, no gel was formed when the concentration of both components was decreased to 1 mg/mL (Figure 1a). A peptide concentration threshold for gelation lies between 5 and 10 mg/mL. When the PAH concentration is fixed at 10 mg/mL, no gel is formed when the Fmoc-FFpY concentration is decreased to 2.5 mg/mL, *i.e.* PAH monomer/Fmoc-FFpY molar ratio equal to 33 (Figure 1b). Decreasing the molecular weight of PAH lead to a less stable gel which was not formed instantaneously. Using PAH with lower molecular weight (Mw = 58 000 g/mol) with PAH monomer/Fmoc-FFpY molar ratio at 8, the gel formed after 24 h and became a viscous solution after the inverted tube test (Figure S1b-c in SI). In the following, PAH/Fmoc-FFpY hydrogels, prepared with PAH monomer/Fmoc-FFpY molar ratio at 8, were studied with PAH (Mw = 120 000 g/mol) unless otherwise stated. PAH/Fmoc-FFpY gel was characterized by oscillatory shear rheometry to determine the shear modulus G' and the storage modulus G" (Figure 2a).

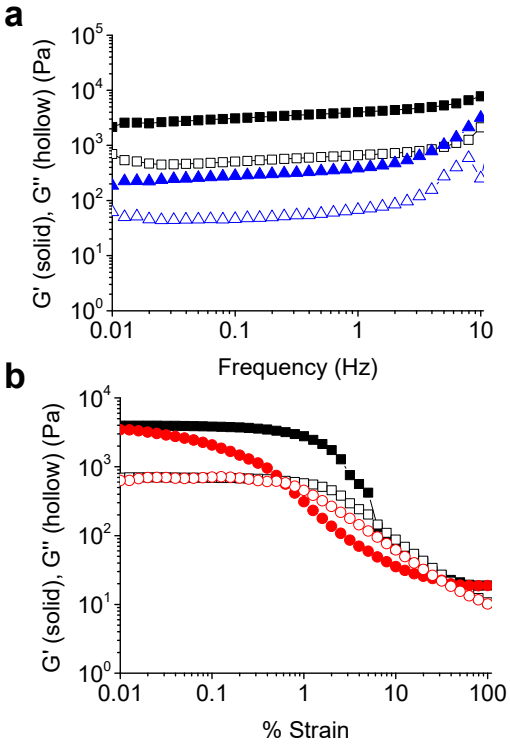

Figure 2. Storage modulus (G' – solid symbols) and loss modulus (G" – hollow symbols) of (a) PAH/Fmoc-FFpY (■) and Fmoc-FFY (▲) hydrogels as a function of the frequency and (b) PAH/Fmoc-FFpY hydrogel as a function of the strain measured from 0.01 to 100% strain (■) and from 100 to 0.01% strain (●) at 25 °C. PAH/Fmoc-FFpY hydrogel was obtained by mixing PAH (Mw= 120 000 g/mol) and Fmoc-FFpY at 10 mg/mL. Fmoc-FFY hydrogel was obtained by mixing AP at 1.5 mg/mL and Fmoc-FFpY at 10 mg/mL.

G' is higher than G" over the frequency range meaning that a gel is formed and remains stable. G' (G") is of the order of 4.2 kPa (0.7 kPa) at a frequency of 1 Hz (strain 0.1%). Obtained at the same peptide concentration using 1.5 mg/mL AP, Fmoc-FFY gels have a G' (G") of 0.4 kPa (0.07 kPa) (Figures 2a and S2 in SI). In comparison, Fmoc-FF gels prepared by dissolution in DMSO followed by water dilution can reach a G' of 300 kPa at high peptide volume fraction.[26, 50] Kinetically con-

trolled self-assembly of Fmoc-FF using pH change induces a slower hydrogelation producing more homogeneous gels with low moduli, G' (G") being between 2 to 400 Pa (1.5 to 90 Pa).[28, 51] The controlled self-assembly can be obtained either through steps of controlled temperature,[28] by Fmoc-FF colloid decomposition or mild change of pH.[51] Non-controlled self-assembly of the peptide gives rise to gels with higher moduli,[17, 25] explained by kinetically trapped aggregates.[28] The gelation of PAH/Fmoc-FFpY is fast due to electrostatic interactions which is the driving force of the self-assembly. This fast process leads probably to kinetically trapped aggregates and thus to higher mechanical properties than Fmoc-FFY hydrogels produced enzymatically by peptide dephosphorylation. No change of turbidity, mechanical properties and structural differences of PAH/Fmoc-FFpY gels were observed even 6 days after the gelation which means that the gel is equilibrated and any aging effect can be predicted (Figure S3 in SI). When keeping the frequency fixed at 1 Hz and varying the strain, both G' and G" remain constant up to a strain of 1% and then decrease when strain is further increased (Figure 2b). When returning continuously to small strains, a hysteresis in G' and G" is observed with a recovery at low strains. At high strains, the gel disrupts and becomes almost liquid like whereas at low strains, it recovers its initial properties, as expected for a supramolecular hydrogel. The supramolecular self-assembly of peptide was visualized by confocal scanning microscopy Thioflavine T, a non-fluorescent probe which becomes fluorescent green when incorporated into self-assemblies rich in β-sheets.[52] Rhodaminated PAH (PAHr) was used to localize PAH in the hydrogel. Homogeneous distributions of red and green fluorescence, coming from PAHr and Thioflavine T respectively, are observed around the sample (Figure 3a). Both fluorescence signals are overlapped, appearing as long, large fibers with PAHr and Fmoc-FFpY at 5 mg/mL. Keeping the molar ratio of PAH monomer/Fmoc-FFpY constant at 8, a homogeneous density of small fibers is seen at lower concentration, *i.e.* 0.5 mg/mL. This explains why PAH/Fmoc-FFpY hydrogels formed with low concentration of PAH and Fmoc-FFpY are less robust.

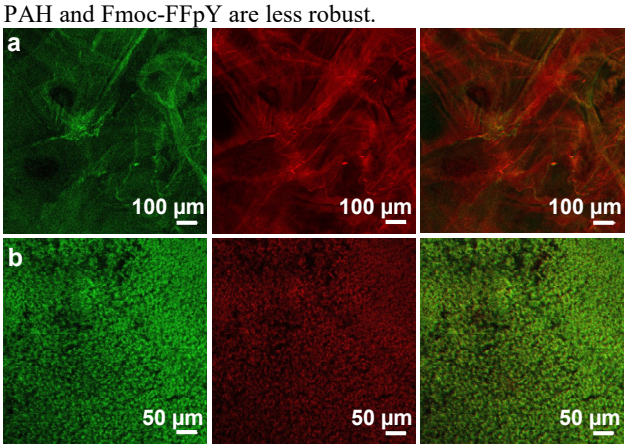

Figure 3. Confocal images, green (left), red (center) and merged (right) channels, of PAH/Fmoc-FFpY hydrogels were obtained in the presence of 1 mg/mL Thioflavin T by mixing (a) 5 mg/mL PAHr and 5 mg/mL Fmoc-FFpY and (b) 0.5 mg/mL PAHr and 0.5 mg/mL Fmoc-FFpY.

Fluorescence of Thioflavine T is not observed in the case of Fmoc-FFpY or PAHr solutions (Figure S4a-b in SI). In comparison, Fmoc-FFY gels, obtained by mixing Fmoc-FFpY and rhodaminated AP, present a completely different morphology with heterogeneous distribution of Thioflavine T and homogeneous distribution of rhodaminated AP (Figure S4c in SI). The self-assembly of PAH/Fmoc-FFpY is homogeneous throughout the whole gel with a colocalization of the tripeptide and the polycation. This suggests that PAH is integral to the self-assembly of Fmoc-FFpY.

Conditions of formation and stability of the gel. Using HPLC, it was shown that Fmoc-FFpY is not dephosphorylated in the presence of PAH (Figure S5 in SI). The formation of the gel must rely on electrostatic interactions between positively charged amine groups of PAH and negatively charged phosphate groups of Fmoc-FFpY. In the presence of *para*-nitrophenyl phosphate (PNP), a competitor bearing a phosphate group, no gel was formed between PAH and Fmoc-FFpY (Figure 4a). In this case, the phosphate groups of Fmoc-FFpY do not interact strongly enough with PAH to form a gel.

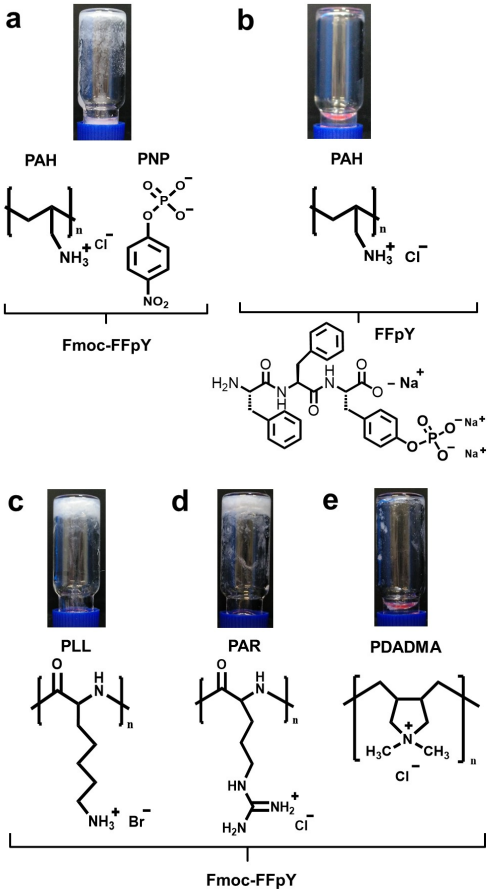

Figure 4. Inverted vial tests, with chemical structures, of (a) PAH (Mw = 120 000 g/mol)/PNP, PNP in an equimolar ratio (1:1) with PAH monomer, added to Fmoc-FFpY solution and (b) PAH (Mw = 120 000 g/mol) added to FFpY solution. (c) PLL (Mw=52 000 g/mol), (d) PAR (Mw = 9 600 g/mol) and (e) PDADMA (Mw=100 000 g/mol) were added to Fmoc-FFpY solution. Solutions were prepared with 107.5 mM polycation monomer and 12.9 mM Fmoc-FFpY (or FFpY), leading to a polycation monomer/Fmoc-FFpY molar ratio of 8.

In the presence of 2 M NaCl, the mixture of PAH and Fmoc-FFpY lead to some aggregates, no consistent hydrogel was obtained (Figure S6a in SI) due to weak electrostatic interaction between PAH and the peptide. These two results point towards the importance of the electrostatic interactions between phosphate groups of tripeptide and primary amine

groups of PAH. The Fmoc moiety of the peptide is also essential. Indeed, mixing PAH with FFpY did not lead to a gel (Figure 4b). Next, the possibility of gel formation with other polycations was checked. Keeping the polycation monomer/Fmoc-FFpY molar ratio at 8, PAH was replaced by PLL bearing primary amines, PAR bearing secondary amines and PDADMA bearing quaternary ammoniums. Whereas gels formed with PLL and PAR (Figures 4c-d), no gel could be observed with PDADMA (Figure 4e). The rigidity of PDADMA chains could explain the absence of gel formation by preventing the self-assembly of Fmoc-FFpY. Indeed, PDADMA[53] has a higher intrinsic persistent length (3 nm) in comparison to PAH or PLL(~1 nm at basic pH).[54-55] The gelation cannot be obtained at pH 7.4, pH 4 or pH 1. With a pKa of 8.5 with a large transition,[56] PAH chains have 30% of protonated amine moieties at pH 9.5. Phosphate groups, from tyrosine phosphate, presents two negative charges at pH 9.5, the second deprotonation pKa being around 6.[57] It seems that a specific balance of protonated/non-protonated amines and phosphate groups is required to obtain a gel.The stability of PAH/Fmoc-FFpY hydrogels was studied, after formation, against the change of temperature or pH and the presence of PNP or AP. The gels remains stable when the temperature was gradually heated up to 70 °C (Figure S6b in SI), as it is usual for electrostatically crosslinked hydrogels. Decreasing the pH from 9.5 to 1.0 also did not affect the stability of the PAH/Fmoc-FFpY hydrogels even if the gel cannot be prepared at this acidic pH (Figure S6c in SI). The addition of PNP (in an equimolar ratio with PAH monomer) caused partial dissolution of PAH/Fmoc-FFpY hydrogel due to competitive PNP/PAH electrostatic interactions (Figure S6d in SI). When an AP (50 µL, 1 mg/mL) solution was added to PAH/Fmoc-FFpY gel (300 µL in volume) for 1 h, dissolution and degradation of the mechanical properties of the gel were observed with G' and G" decreasing to 0.85 and 0.32 kPa, respectively (Figure S6e and S7a in SI). The dephosphorylation of Fmoc-FFpY by AP broke the electrostatic interaction between the phosphate moieties of the tripeptides and amine groups of PAH. PAH/Fmoc-FFpY gels were stable over at least 6 days in the presence of RPMI cell culture medium (pH 7.0 – 7.6) (Figure S6f in SI) and showed an increase of its mechanical properties, reaching G' (G") of 6.3 kPa (1.2 kPa) at a frequency of 1 Hz (strain 0.1%) (Figure S7b in SI). These results allow its use for *in-vivo* applications.

Secondary structure of PAH/Fmoc-FFpY gel. FTIR spectroscopy was employed to compare the secondary structure of self-assembled Fmoc-FFpY induced by PAH with self-assembled Fmoc-FFY obtained by dephosphorylation of Fmoc-FFpY by AP (Figure 5a). The spectrum of Fmoc-FFpY in deuterated solvent shows a broad amide I band centered at 1645 cm^{-1}, attributed to unstacked amide groups,[58] a broad carboxylate vibrational band at 1594 cm^{-1}, assigned to the deprotonated form of the terminal carboxylic acid groups,[28] and a peak centered at 1685 cm^{-1}, assigned to the carbamate moiety[59]. In the case of PAH/Fmoc-FFpY hydrogel, a broadening of the amide I band is observed with the appearance of a peak at 1630 cm^{-1} attributed to the β-sheet structure with higher intensity than the peak at 1645 cm^{-1} attributed to the unstacked amide I. The carbamate peak is shifted to 1685 cm^{-1} which is also consistent with a β-sheet structure and a possible anti-parallel arrangement. The broad contribution of the carboxylate peak at 1584 cm^{-1} indicates that terminal carboxylic acid groups remain deprotonated.[28]To gain further structural insight, the amide I band was decomposed to identify the contributions of the secondary structures adopted by the peptides in both types of hydrogel (Figure S8-9 in SI). The relative contributions of the different secondary structures to the amide I band of PAH/Fmoc-FFpY and Fmoc-FFY hydrogels are summarized in Table S1 in SI. PAH/Fmoc-FFpY gels present 54% β-sheets (with 3% of antiparallel β-sheets), 41% random structures and 5% of α-helices. In contrast, Fmoc-FFY gels present 59% random structure and 41% β-sheets (with 15% of antiparallel β-sheets).

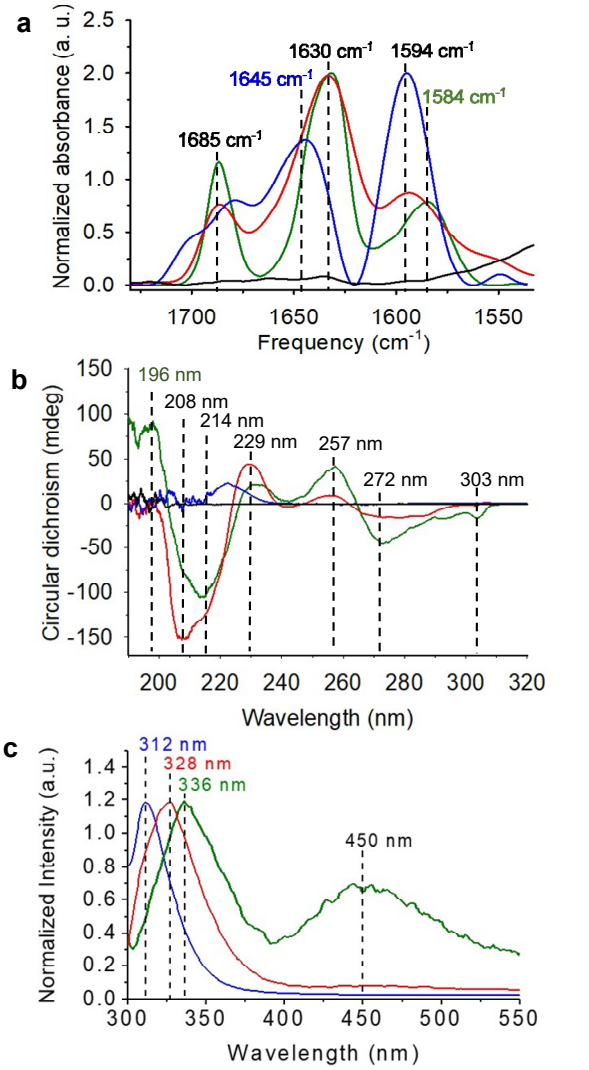

Figure 5. (a) ATR-FTIR (b) Fluorescence emission (λ_{ex}=290 nm) and (c) CD spectra of PAH/Fmoc-FFpY (green curve), AP/Fmoc-FFpY mixture (red curve), Fmoc-FFpY (blue curve), and PAH (black curve). In the case of FTIR experiments, the solutions were prepared in deuterated buffer.

The structural organization of Fmoc-FFpY in PAH/Fmoc-FFpY gels was further investigated by circular dichroism (CD) (Figure 5b). In agreement with FTIR results, the CD spectrum of PAH/Fmoc-FFpY hydrogel presents the signature of β-sheets structures, with a positive band at 196 nm and a strong negative band at 214 nm.[25] The CD spectrum of PAH/Fmoc-FFpY also presents negative bands at 272 nm and 303 nm, attributed to offset face-to-face stacking of the Fmoc moieties and the fluorenyl absorption, respectively.[24] The presence of

two maxima at 229 and 257 nm is a signature of stacking interactions of the aromatic units of Fmoc-FFpY.[60] The CD spectrum of AP/Fmoc-FFpY hydrogel is very similar to that of PAH/Fmoc-FFpY, except for the disappearance of the positive peak at 196 nm and the shifting of the strong negative peak to lower wavelengths, which is close to the signature of random structure, also in agreement with FTIR. Fluorescence spectroscopy was used to check the excimer formation of Fmoc moieties after Fmoc-peptide self-assembly.[22, 27] When irradiated at 290 nm, Fmoc-FFpY solutions present a fluorescence emission at 310 nm due to fluorenyl moieties. The presence of AP, leading to self-assembly of Fmoc-FFY, induces a shift of this peak from 310 nm towards 328 nm, due to fluorenyl excimers (Figure 5c). For PAH/Fmoc-FFpY solution, the fluorescence peak shift towards 336 nm is almost instantaneous after mixing while it is more gradual with AP. In the case of PAH, the self-assembly takes place almost instantaneously because it is driven by electrostatic interactions while in the case of AP, the self-assembly results from dephosphorylation of Fmoc-FFpY which is a slower process. In the case of PAH/Fmoc-FFpY hydrogels, a broad band with a maximum at 450 nm is observed which could indicate the presence of J-aggregates formed by multiple aromatic groups, including phenyl and fluorenyl rings, stacked through π-π interactions.[25, 27] In this case, the fluorenyl groups overlap more efficiently and move less freely in PAH/Fmoc-FFpY hydrogel.[61]

Structural study of PAH/Fmoc-FFpY gel. TEM images of PAH/Fmoc-FFpY gels, obtained by mixing 5 mg/mL PAH and 5 mg/mL Fmoc-FFpY, show a homogeneous density of thin fibers, 9 nm in width, from 200 to 800 nm in length (Figure S10a in SI). Isolated and pairs of fibers are visible (Figures 6a). In comparison, Fmoc-FFY hydrogels display long fibers, 10 nm in width, several micrometers in length (Figure S10b in SI). Small- and wide-angle X-ray scattering experiments (SAXS-WAXS) were performed as complementary measurements to TEM. For well-defined scattering objects, SAXS allows probing the shape and the size of nano-objects and WAXS their internal structure at the molecular scale. The scattered intensity from PAH/Fmoc-FFpY gel is completely different from that of pure Fmoc-FFpY or pure PAH and reveals a particular self-assembled association. Two different q-ranges can be identified (Figure 6b).

.

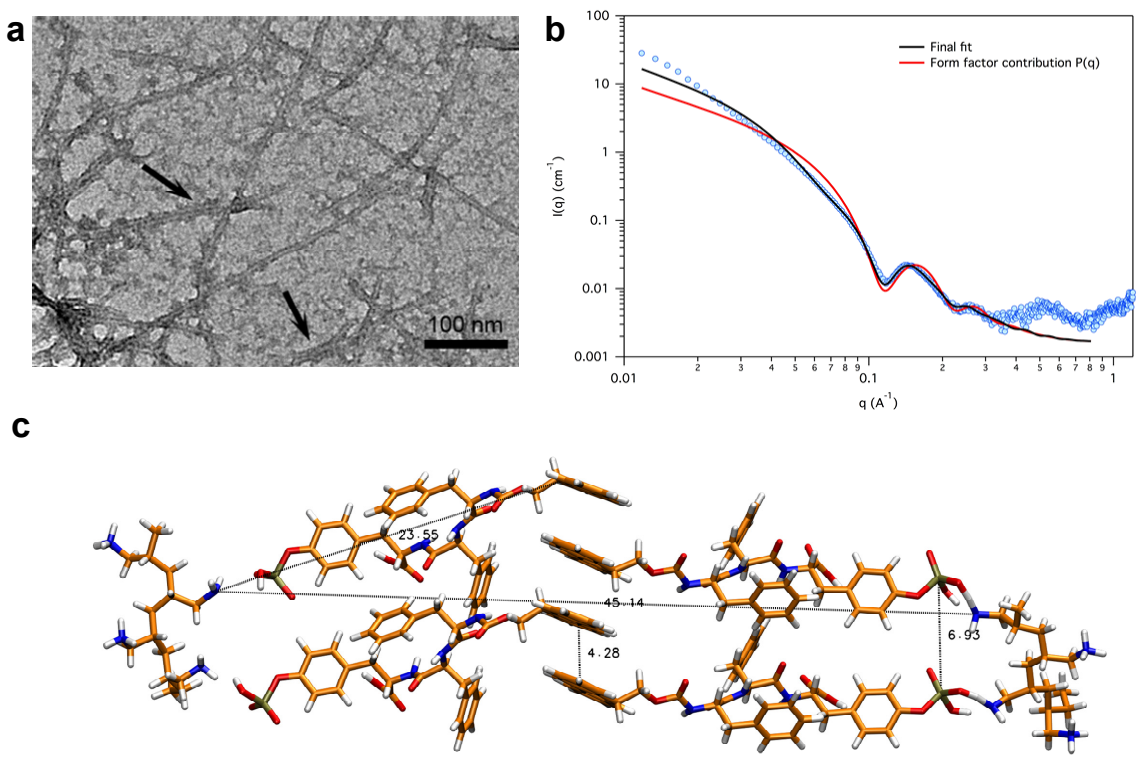

Figure 6. (a) TEM image, after negative staining, of PAH/Fmoc-FFpY hydrogel showing individual fibers. These fibers associate to form pairs as indicated by the black arrows. (b) SAXS and WAXS intensities (cm^{-1}) of PAH/Fmoc-FFpY hydrogel. Black curve: fit with an associated core-shell cylinders model (Φ = 0.065, R_1 = 29.1 Å, R_2 = 22.8 Å, ρ_1 = 11.47 10^{10} cm^{-2}, ρ_2 = 10.29 10^{10} cm^{-2}, ρ_s = 9.40 10^{10} cm^{-2}, Δ_2 = 3 Å, bkg = 0.0017 cm^{-1}). Red curve: contribution of the form factor P(q) to the final fit. The fit was performed on a restricted q-range centered on the characteristic oscillations (0.145 and 0.26 $Å^{-1}$). The hydrogels were obtained at 5 mg/mL PAH (Mw= 120 000 g/mol) and 5 mg/mL Fmoc-FFpY concentrations. (c) Geometry optimized structure of PAH/Fmoc-FFpY cluster. Note: On the right side of the optimized structure, the calculation in gas phase induces the establishment of a proton transfer between the amino group of PAH and one of the oxygen of the phosphate group of Fmoc-FFpY. This is inherent to the fact that calculations have been performed in the gas phase (without water). However, we believe that this has no impact on the conclusion we have drawn from these calculations.

From 0.010 to 0.35 $Å^{-1}$ (SAXS region), a large decrease in intensity is observed while two maxima are present around 0.145 and 0.26 $Å^{-1}$. This behavior is related to the presence of large and well-defined scattering objects in the solution and

can be interpreted on the basis of geometrical models described in Materials and Methods. Between 0.35 and 1 $Å^{-1}$ (WAXS region), smaller distances are probed where two large maxima, at 0.54 and 0.95 $Å^{-1}$, corresponding to typical distances of the order of 12 and 6-7 Å, respectively, are observed and linked to the internal structure of the nano-objects. Only a restricted q-range in the SAXS region centered on the characteristic oscillations (0.145 and 0.26 $Å^{-1}$) was considered and analyzed using theoretical form factors based on cylindrical nano-objects. This fitting procedure was chosen based on the fact that well defined isolated and pairs of parallel fibers were observed by TEM. The scattered intensity at very low q (SAXS region), probably and partially related to the presence of large bundles of nano-objects (observed by TEM) (Figure S10a in SI), was not considered in the fitting procedure. As the typical length of the fibers (from 200 to 800 nm) are too large to be observed directly by SAXS, infinitely long cylinders were considered for the fit. Different models were tested: single cylinders, associated cylinders, single core-shell cylinders and associated core-shell cylinders. The final fits of each model are given in Figures S11-S14 in SI. Single and associated cylinders models cannot explain the specific intensity variation below 0.1 $Å^{-1}$. Finally, only the associated core-shell cylinders model is able to reproduce the data (Figure 6b) with a slight underestimation of the intensity below 0.02 $Å^{-1}$. This effect may be due to the presence of large heterogeneities in the sample (bundles of fibers) which were not taken into account in the analysis. In this model, the core-shell cylinders tend to assemble together forming pairs of parallel fibers. The two maxima observed between 0.1 and 0.3 $Å^{-1}$ are associated to the first oscillations of the form factor and are characteristic of the well-defined geometry of the fibers. The association of the cylinders affects their shape, being responsible for the strong asymmetric profile observed on the first oscillation (0.145 $Å^{-1}$). Core-shell cylinders have an average core radius R_2 = 23 ± 3 Å, with a small polydispersity, and an external radius R_1 = 29 Å. The shell thickness e is close to 6 Å ($e = R_1 - R_2$). The external diameter (5.8 nm) is in agreement with the value (9 nm) observed by TEM measurements, since negative staining always tends to overestimate diameters. The scattering length density of the core ($\rho_2 = 10.29\ 10^{10}\ cm^{-2}$) is smaller than that of the shell ($\rho_1 = 11.47\ 10^{10}\ cm^{-2}$). The nature of the core and the shell are directly linked to a spatial organization of PAH and Fmoc-FFpY in the fibers. Similarly to polyelectrolytes/oppositely charge surfactants systems, PAH/Fmoc-FFpY mixture may lead to the formation of complexes in which flexible polyions (shell) decorate micellar aggregates (core). In order to validate this scenario and more particularly the characteristic distances determined by SAXS, geometry optimization was performed in the gas phase on a very simple system (Figure 6c). Fmoc-FFpY were organized through fluorenyl stacking, thanks to π–π interactions, decorated at the other extremity by PAH chains, due to electrostatic interactions with phosphate groups. The spatial organization of PAH and Fmoc-FFpY shows typical distances that are compatible with the core-shell description. In particular, the distance (45 Å) between two chains of PAH, separated by stacked Fmoc-FFpY reproduces the diameter of the core (46 Å) and the PAH backbone diameter, of the order of 5-6 Å, the shell thickness (6 Å). The WAXS region with the two large maxima at 0.54 and 0.95 $Å^{-1}$ (~12 and ~6-7 Å) provides information on the internal peptide organization within the cylindrical self-assembly. Characteristic reflections associated with β-sheet organization are often found for peptides around ~1.3 $Å^{-1}$ (4.8 Å) and ~0.63 $Å^{-1}$ (10.5 Å).[62] They are linked to the distance between hydrogen-bonded backbones in the β-sheets and the distance between two β-sheets respectively, and can change slightly according to the nature of the peptides. In PAH/Fmoc-FFpY mixtures, only the first characteristic peak (~0.6 $Å^{-1}$) seems to be observed, but its average position is displaced to smaller q values (~0.54 $Å^{-1}$, ~12 Å) while its broadening is increased. The second characteristic reflection (1.3 $Å^{-1}$, 4.8 Å) is absent probably because of a very poor signal/background ratio in this q-range (the scattering of the solvent is much larger than that of the particle). We instead observe a small contribution around 0.95 $Å^{-1}$ (6-7 Å). The simple geometry optimization is not intended to reproduce accurately the real 3D molecular organization within the cylindrical objects or the secondary structure of the self-assembly but rather to support the typical distances determined by fitting SAXS curves. The typical distances between Fmoc molecules along the vertical axis (cylinder axis) and its phenyl moieties are in between 7 and 9 Å, close to the experimental values.

Conclusions

Phosphorylated Fmoc-FF based peptides are widely used to form self-assembled structures which yield hydrogels following enzymatic dephosphorylation. Here, we show that mixing them with polycations also leads to gel formation through interaction between the phosphate groups of Fmoc-FFpY and the charged amine groups along the polycation backbone. Conditions for PAH/Fmoc-FFpY gelation were investigated, the self-assembly between the peptide groups was demonstrated, the rheological properties of the resulting gel were determined and the morphological properties of the gel were studied in detail. TEM experiments show the presence of fibers whose fine structure was investigated by SAXS and WAXS. The geometrical factors characterizing the fibers obtained by SAXS are in agreement with typical distances obtained by gas phase geometry optimization. This work widens the possible applications, in particular as injectable biomaterials, of Fmoc-tripeptides whose self-assembly is usually triggered by a change of solvent, pH, temperature or enzymatically. Moreover, the use of specific polycations could endow the hydrogels with antimicrobial properties.

ASSOCIATED CONTENT

Supporting Information

The following files are available free of charge. Phase diagram, , rheological measurements of Fmoc-FFY hydrogels, PAH/Fmoc-FFpY after 6 days and in contact with culture medium, confocal images of Fmoc-FFY hydrogel and control experiments, HPLC graphs PAH/Fmoc-FFpY, Fmoc-FFpY and Fmoc-FFY, inverted tube tests under several conditions for stability tests, FTIR decomposition of the amide I band of Fmoc-FFY hydrogels and PAH/Fmoc-FFpY, TEM images of the PAH/Fmoc-FFpY and Fmoc-FFY hydrogels, SAXS fits of PAH/Fmoc-FFpY hydrogel using different geometrical models.

AUTHOR INFORMATION

Corresponding Author

* Fouzia Boulmedais E-mail: fouzia.boulmedais@ics-cnrs.unistra.fr; phone: +33-3-88-41-41-60. Pierre Schaaf E-mail: schaaf@unistra.fr; phone: +33-3-68-85-33-87

Author Contributions

The manuscript was written through contributions of all authors. / All authors have given approval to the final version of the manuscript. / ‡These authors contributed equally.

ACKNOWLEDGMENT

J.R.F. acknowledges International Center for Frontier Research in Chemistry (Labex CSC, PSC-016 and PSC-005) for PhD fellowship. J.B.S. thanks the France-USA Fulbright commission. ICS microscopy platform is acknowledged for the use of the TEM instrument. We gratefully acknowledge the financial supports from Agence Nationale de la Recherche (EASA, ANR-18-CE06-0025-03) and Institut Carnot MICA (DIAART).

REFERENCES

(1) Wu, Q.; He, Z.; Wang, X.; Zhang, Q.; Wei, Q.; Ma, S.; Ma, C.; Li, J.; Wang, Q. Cascade Enzymes within Self-Assembled Hybrid Nanogel Mimicked Neutrophil Lysosomes for Singlet Oxygen Elevated Cancer Therapy. *Nat. Commun.* **2019,** *10*, 240.

(2) Alakpa, E. V.; Jayawarna, V.; Lampel, A.; Burgess, K. V.; West, C. C.; Bakker, S. C. J.; Roy, S.; Javid, N.; Fleming, S.; Lamprou, D. A.; Yang, J. L.; Miller, A.; Urquhart, A. J.; Frederix, P. W. J. M.; Hunt, N. T.; Peault, B.; Ulijn, R. V.; Dalby, M. J. Tunable Supramolecular Hydrogels for Selection of Lineage-Guiding Metabolites in Stem Cell Cultures. *Chem.* **2016,** *1*, 298-319.

(3) Boekhoven, J.; Poolman, J. M.; Maity, C.; Li, F.; van der Mee, L.; Minkenberg, C. B.; Mendes, E.; van Esch, J. H.; Eelkema, R. Catalytic Control over Supramolecular Gel Formation. *Nat. Chem.* **2013,** *5*, 433.

(4) Rodon Fores, J.; Criado-Gonzalez, M.; Chaumont, A.; Carvalho, A.; Blanck, C.; Schmutz, M.; Serra, C. A.; Boulmedais, F.; Schaaf, P.; Jierry, L. Supported Catalytically-Active Supramolecular Hydrogels for Continuous Flow Chemistry. *Angew. Chem. Int. Ed.* **2019,** *58*, 1-7.

(5) Rodon Fores, J.; Criado-Gonzalez, M.; Schmutz, M.; Blanck, C.; Schaaf, P.; Boulmedais, F.; Jierry, L. Protein-Induced Low Molecular Weight Hydrogelator Self-Assembly through a Self-Sustaining Process. *Chem. Sci.* **2019,** *10*, 4761-4766.

(6) Li, Y.; Wang, F. H.; Cui, H. G. Peptide-Based Supramolecular Hydrogels for Delivery of Biologics. *Bioeng Transl Med* **2016,** *1*, 306-322.

(7) Branco, M. C.; Schneider, J. P. Self-Assembling Materials for Therapeutic Delivery. *Acta Biomater.* **2009,** *5*, 817-831.

(8) Lehn, J. M. From Molecular to Supramolecular Chemistry. In *Supramolecular Chemistry*, Lehn, J. M., Ed.; VCH: Weinheim, 1995; Chapter 1; pp. 1-9.

(9) Mattia, E.; Otto, S. Supramolecular Systems Chemistry. *Nat. Nanotechnol.* **2015,** *10*, 111–119.

(10) Lehn, J.-M. Perspectives in Chemistry—Aspects of Adaptive Chemistry and Materials. *Angew. Chem. Int. Ed.* **2015,** *54*, 3276-3289.

(11) Gyarmati, B.; Szilagyi, B. A.; Szilagyi, A. Reversible Interactions in Self-Healing and Shape Memory Hydrogels. *Eur. Polym. J.* **2017,** *93*, 642-669.

(12) Wang, T.; Jones, J. D.; Niyonshuti, I. I.; Agrawal, S.; Gundampati, R. K.; Suresh Kumar, T. K.; Quinn, K. P.; Chen, J. Biocompatible, Injectabke Anionic Hydrogels Based on Poly(Oligo Ethylene Glycol Monoacrylate-Co-Acrylic Acid) for Protein Delivery. *Adv. Therap.* **2019**, 1900092.

(13) Du, X.; Zhou, J.; Shi, J.; Xu, B. Supramolecular Hydrogelators and Hydrogels: From Soft Matter to Molecular Biomaterials. *Chem. Rev.* **2015,** *115*, 13165-13307.

(14) Collier, J. H.; Hu, B. H.; Ruberti, J. W.; Zhang, J.; Shum, P.; Thompson, D. H.; Messersmith, P. B. Thermally and Photochemically Triggered Self-Assembly of Peptide Hydrogels. *J. Am. Chem. Soc.* **2001,** *123*, 9463-9464.

(15) Chen, L.; Pont, G.; Morris, K.; Lotze, G.; Squires, A.; Serpell, L. C.; Adams, D. J. Salt-Induced Hydrogelation of Functionalised-Dipeptides at High Ph. *Chem. Commun.* **2011,** *47*, 12071-12073.

(16) Aggeli, A.; Bell, M.; Carrick, L. M.; Fishwick, C. W. G.; Harding, R.; Mawer, P. J.; Radford, S. E.; Strong, A. E.; Boden, N. Ph as a Trigger of Peptide B-Sheet Self-Assembly and Reversible Switching between Nematic and Isotropic Phases. *J. Am. Chem. Soc.* **2003,** *125*, 9619-9628.

(17) Mahler, A.; Reches, M.; Rechter, M.; Cohen, S.; Gazit, E. Rigid, Self-Assembled Hydrogel Composed of a Modified Aromatic Dipeptide. *Adv. Mater.* **2006,** *18*, 1365-1370.

(18) Zhao, F.; Gao, Y.; Shi, J.; Browdy, H. M.; Xu, B. Novel Anisotropic Supramolecular Hydrogel with High Stability over a Wide Ph Range. *Langmuir* **2011,** *27*, 1510-1512.

(19) Bowerman, C. J.; Nilsson, B. L. A Reductive Trigger for Peptide Self-Assembly and Hydrogelation. *J. Am. Chem. Soc.* **2010,** *132*, 9526-9527.

(20) Yang, Z.; Gu, H.; Fu, D.; Gao, P.; Lam, J. K.; Xu, B. Enzymatic Formation of Supramolecular Hydrogels. *Adv. Mater.* **2004,** *16*, 1440-1444.

(21) Yang, Z.; Xu, B. Using Enzymes to Control Molecular Hydrogelation. *Adv. Mater.* **2006,** *18*, 3043-3046.

(22) Criado-Gonzalez, M.; Rodon Fores, J.; Wagner, D.; Schröder, A. P.; Carvalho, A.; Schmutz, M.; Harth, E.; Schaaf, P.; Jierry, L.; Boulmedais, F. Enzyme-Assisted Self-Assembly within a Hydrogel Induced by Peptide Diffusion. *Chem. Commun.* **2019,** *55*, 1156-1159.

(23) Makam, P.; Gazit, E. Minimalistic Peptide Supramolecular Co-Assembly: Expanding the Conformational Space for Nanotechnology. *Chem. Soc. Rev.* **2018,** *47*, 3406-3420.

(24) Ryan, D. M.; Anderson, S. B.; Senguen, F. T.; Youngman, R. E.; Nilsson, B. L. Self-Assembly and Hydrogelation Promoted by F5-Phenylalanine. *Soft Matter* **2010,** *6*, 475-479.

(25) Smith, A. M.; Williams, R. J.; Tang, C.; Coppo, P.; Collins, R. F.; Turner, M. L.; Saiani, A.; Ulijn, R. V. Fmoc-Diphenylalanine Self Assembles to a Hydrogel Via a Novel Architecture Based on Π–Π Interlocked B-Sheets. *Adv. Mater.* **2008,** *20*, 37-41.

(26) Dudukovic, N. A.; Zukoski, C. F. Mechanical Properties of Self-Assembled Fmoc-Diphenylalanine Molecular Gels. *Langmuir* **2014,** *30*, 4493-4500.

(27) Tang, C.; Ulijn, R. V.; Saiani, A. Effect of Glycine Substitution on Fmoc–Diphenylalanine Self-Assembly and Gelation Properties. *Langmuir* **2011,** *27*, 14438-14449.

(28) Tang, C.; Smith, A. M.; Collins, R. F.; Ulijn, R. V.; Saiani, A. Fmoc-Diphenylalanine Self-Assembly Mechanism Induces Apparent Pka Shifts. *Langmuir* **2009,** *25*, 9447-9453.

(29) Vigier-Carrière, C.; Wagner, D.; Chaumont, A.; Durr, B.; Lupattelli, P.; Lambour, C.; Schmutz, M.; Hemmerlé, J.; Senger, B.; Schaaf, P.; Boulmedais, F.; Jierry, L. Control of Surface-Localized, Enzyme-Assisted Self-Assembly of Peptides through Catalyzed Oligomerization. *Langmuir* **2017,** *33*, 8267-8276.

(30) Criado-Gonzalez, M.; Fores, J. R.; Carvalho, A.; Blanck, C.; Schmutz, M.; Kocgozlu, L.; Schaaf, P.; Jierry, L.; Boulmedais, F. Phase Separation in Supramolecular Hydrogels Based on Peptide Self-Assembly from Enzyme-Coated Nanoparticles. *Langmuir* **2019,** *35*, 10838-10845.

(31) Boothroyd, S.; Saiani, A.; Miller, A. F. Controlling Network Topology and Mechanical Properties of Co-Assembling Peptide Hydrogels. *Biopolymers* **2014,** *101*, 669-680.

(32) Radvar, E.; Azevedo, H. S. Supramolecular Peptide/Polymer Hybrid Hydrogels for Biomedical Applications. *Macromol. Biosci.* **2019,** *19*, 1800221.

(33) Capito, R. M.; Azevedo, H. S.; Velichko, Y. S.; Mata, A.; Stupp, S. I. Self-Assembly of Large and Small Molecules into Hierarchically Ordered Sacs and Membranes. *Science* **2008,** *319*, 1812-1816.

(34) Ferreira, D. S.; Marques, A. P.; Reis, R. L.; Azevedo, H. S. Hyaluronan and Self-Assembling Peptides as Building Blocks to Reconstruct the Extracellular Environment in Skin Tissue. *Biomater. Sci.* **2013,** *1*, 952-964.

(35) Mendes, A. C.; Smith, K. H.; Tejeda-Montes, E.; Engel, E.; Reis, R. L.; Azevedo, H. S.; Mata, A. Co-Assembled and Microfabricated Bioactive Membranes. *Adv. Funct. Mater.* **2013,** *23*, 430-438.

(36) Rozkiewicz, D. I.; Myers, B. D.; Stupp, S. I. Interfacial Self-Assembly of Cell-Like Filamentous Microcapsules. *Angew. Chem. Int. Ed.* **2011,** *50*, 6324-6327.

(37) Boekhoven, J.; Zha, R. H.; Tantakitti, F.; Zhuang, E.; Zandi, R.; Newcomb, C. J.; Stupp, S. I. Alginate-Peptide Amphiphile Core-Shell Microparticles as a Targeted Drug Delivery System. *RSC Adv.* **2015,** *5*, 8753-8756.

(38) Radvar, E.; Azevedo, H. S. Supramolecular Nanofibrous Peptide/Polymer Hydrogels for the Multiplexing of Bioactive Signals. *ACS Biomater. Sci. Eng.* **2019,** *5*, 4646-4656.

(39) Fernandez-Muinos, T.; Recha-Sancho, L.; Lopez-Chicon, P.; Castells-Sala, C.; Mata, A.; Semino, C. E. Bimolecular Based Heparin and Self-Assembling Hydrogel for Tissue Engineering Applications. *Acta Biomater.* **2015,** *16*, 35-48.

(40) Kumar, V. A.; Shi, S.; Wang, B. K.; Li, I. C.; Jalan, A. A.; Sarkar, B.; Wickremasinghe, N. C.; Hartgerink, J. D. Drug-Triggered and Cross-

Linked Self-Assembling Nanofibrous Hydrogels. *J. Am. Chem. Soc.* **2015,** *137*, 4823-4830.
(41) Abbas, M.; Xing, R. R.; Zhang, N.; Zou, Q. L.; Yan, X. H. Antitumor Photodynamic Therapy Based on Dipeptide Fibrous Hydrogels with Incorporation of Photosensitive Drugs. *ACS Biomater. Sci. Eng.* **2018,** *4*, 2046-2052.
(42) Xing, R. R.; Li, S. K.; Zhang, N.; Shen, G. Z.; Mohwald, H.; Yan, X. H. Self-Assembled Injectable Peptide Hydrogels Capable of Triggering Antitumor Immune Response. *Biomacromolecules* **2017,** *18*, 3514-3523.
(43) Mertz, D.; Hemmerle, J.; Boulmedais, F.; Voegel, J. C.; Lavalle, P.; Schaaf, P. Polyelectrolyte Multilayer Films under Mechanical Stretch. *Soft Matter* **2007,** *3*, 1413-1420.
(44) Fleissner, G.; Hage, W.; Hallbrucker, A.; Mayer, E. Improved Curve Resolution of Highly Overlapping Bands by Comparison of Fourth-Derivative Curves. *Appl. Spectrosc.* **1996,** *50*, 1235-1245.
(45) Kline, S. R. Reduction and Analysis of Sans and Usans Data Using Igor Pro. *J. Appl. Crystallogr.* **2006,** *39*, 895-900.
(46) Hanwell, M. D.; Curtis, D. E.; Lonie, D. C.; Vandermeersch, T.; Zurek, E.; Hutchison, G. R. Avogadro: An Advanced Semantic Chemical Editor, Visualization, and Analysis Platform. *J. Cheminform.* **2012,** *4*, 17.
(47) Frisch, M. J.; Trucks, G. W.; Schlegel, H. B.; G. E. Scuseria; Robb, M. A.; Cheeseman, J. R.; Scalmani, G.; Barone, V.; Petersson, G. A.; Nakatsuji, H.; Li, X.; Caricato, M.; Marenich, A.; Bloino, J.; Janesko, B. G.; Gomperts, R.; Mennucci, B.; Hratchian, H. P.; Ortiz, J. V.; Izmaylov, A. F.; Sonnenberg, J. L.; Williams-Young, D.; Ding, F.; Lipparini, F.; Egidi, F.; Goings, J.; Peng, B.; Petrone, A.; Henderson, T.; Ranasinghe, D.; Zakrzewski, V. G.; Gao, J.; Rega, N.; Zheng, G.; Liang, W.; Hada, M.; Ehara, M.; Toyota, K.; Fukuda, R.; Hasegawa, J.; Ishida, M.; Nakajima, T.; Honda, Y.; Kitao, O.; Nakai, H.; Vreven, T.; Throssell, K.; Montgomery, J., J. A. ; Peralta, J. E.; Ogliaro, F.; Bearpark, M.; Heyd, J. J.; Brothers, E.; Kudin, K. N.; Staroverov, V. N.; Keith, T.; Kobayashi, R.; Normand, J.; Raghavachari, K.; Rendell, A.; Burant, J. C.; Iyengar, S. S.; Tomasi, J.; Cossi, M.; Millam, J. M.; Klene, M.; Adamo, C.; Cammi, R.; Ochterski, J. W.; Martin, R. L.; Morokuma, K.; Farkas, O.; Foresman, J. B.; Fox, D. J. *Gaussian 09, Revision A.02*, Gaussian, Inc.: Wallingford CT, 2016.
(48) Vigier-Carrière, C.; Garnier, T.; Wagner, D.; Lavalle, P.; Rabineau, M.; Hemmerlé, J.; Senger, B.; Schaaf, P.; Boulmedais, F.; Jierry, L. Bioactive Seed Layer for Surface-Confined Self-Assembly of Peptides. *Angew. Chem. Int. Ed.* **2015,** *54*, 10198-10201.
(49) Raghavan, S. R.; Cipriano, B. H. Gel Formation: Phase Diagrams Using Tabletop Rheologyand Calorimetry. In *Molecular Gels Materials with Self-Assembled Fibrillar Networks*, Weiss, R. G.; Terech, P., Eds.; Springer: Dordrecht, 2005.
(50) Basavalingappa, V.; Guterman, T.; Tang, Y.; Nir, S.; Lei, J.; Chakraborty, P.; Schnaider, L.; Reches, M.; Wei, G.; Gazit, E. Expanding the Functional Scope of the Fmoc-Diphenylalanine Hydrogelator by Introducing a Rigidifying and Chemically Active Urea Backbone Modification. *Adv. Sci.* **2019,** *6*, 1900218.
(51) Ding, B. Y.; Li, Y.; Qin, M.; Ding, Y.; Cao, Y.; Wang, W. Two Approaches for the Engineering of Homogeneous Small-Molecule Hydrogels. *Soft Matter* **2013,** *9*, 4672-4680.
(52) Biancalana, M.; Koide, S. Molecular Mechanism of Thioflavin-T Binding to Amyloid Fibrils. *Bba-Proteins Proteom* **2010,** *1804*, 1405-1412.
(53) Dautzenberg, H.; Gornitz, E.; Jaeger, W. Synthesis and Characterization of Poly(Diallyldimethylammonium Chloride) in a Broad Range of Molecular Weight. *Macromol Chem Physic* **1998,** *199*, 1561-1571.
(54) Cranford, S. W.; Buehler, M. J. Variation of Weak Polyelectrolyte Persistence Length through an Electrostatic Contour Length. *Macromolecules* **2012,** *45*, 8067-8082.
(55) Shi, L.; Carn, F.; Boue, F.; Mosser, G.; Buhler, E. Control over the Electrostatic Self-Assembly of Nanoparticle Semiflexible Biopolyelectrolyte Complexes. *Soft Matter* **2013,** *9*, 5004-5015.
(56) Fang, M. M.; Kim, C. H.; Saupe, G. B.; Kim, H. N.; Waraksa, C. C.; Miwa, T.; Fujishima, A.; Mallouk, T. E. Layer-by-Layer Growth and Condensation Reactions of Niobate and Titanoniobate Thin Films. *Chem. Mater.* **1999,** *11*, 1526-1532.
(57) Bourne, N.; Williams, A. Effective Charge on Oxygen in Phosphoryl (-Po3-2-) Group Transfer from an Oxygen Donor. *J. Org. Chem.* **1984,** *49*, 1200-1204.
(58) Mu, X. J.; Eckes, K. M.; Nguyen, M. M.; Suggs, L. J.; Ren, P. Y. Experimental and Computational Studies Reveal an Alternative Supramolecular Structure for Fmoc-Dipeptide Self-Assembly. *Biomacromolecules* **2012,** *13*, 3562-3571.
(59) Fleming, S.; Frederix, P. W. J. M.; Sasselli, I. R.; Hunt, N. T.; Ulijn, R. V.; Tuttle, T. Assessing the Utility of Infrared Spectroscopy as a Structural Diagnostic Tool for Beta-Sheets in Self-Assembling Aromatic Peptide Amphiphiles. *Langmuir* **2013,** *29*, 9510-9515.
(60) Krysmann, M. J.; Castelletto, V.; Kelarakis, A.; Hamley, I. W.; Hule, R. A.; Pochan, D. J. Self-Assembly and Hydrogelation of an Amyloid Peptide Fragment. *Biochemistry* **2008,** *47*, 4597-4605.
(61) Yang, Z. M.; Gu, H. W.; Zhang, Y.; Wang, L.; Xu, B. Small Molecule Hydrogels Based on a Class of Antiinflammatory Agents. *Chem. Commun.* **2004**, 208-209.
(62) Gobeaux, F.; Wien, F. Reversible Assembly of a Drug Peptide into Amyloid Fibrils: A Dynamic Circular Dichroism Study. *Langmuir* **2018,** *34*, 7180-7191.

SYNOPSIS TOC